GEOPHYSICAL RESEARCH LETTERS

Supporting Information for "The double dip: how tropospheric expansion counteracts increases in extratropical stratospheric ozone under global warming"

A. Match[1], E. P. Gerber[1]

[1]Center for Atmosphere Ocean Science, Courant Institute of Mathematical Sciences, New York University

Contents of this file

1. Text S1 to S2
2. Figures S1 to S6

Introduction

This supplemental information contains an explanation of the Chapman+2 photochemical-transport model, both its formulation (Text S1) and its numerical implementation (Text S2). This supplemental information also includes 6 supplemental figures.

Text S1: Methods: The Chapman+2 model with a three-column leaky tropical pipe

---

We analyze the ozone response to rising CO_2 in an idealized photochemical transport model in which stratospheric cooling, strengthening BDC, and tropospheric expansion can be independently imposed. Our model divides the atmosphere into a tropical column, a Northern Hemisphere (NH) extratropical column, and a Southern Hemisphere (SH) extratropical column. In each column, we integrate seasonally-evolving tendencies in ozone from photochemistry and transport, as follows:

$$\frac{\partial[\mathrm{O_3}]}{\partial t} = \frac{\partial[\mathrm{O_3}]}{\partial t}|_{\mathrm{photochem}} + \frac{\partial[\mathrm{O_3}]}{\partial t}|_{\mathrm{transport}} \tag{1}$$

A schematic of our model domain and its physical processes is shown in Fig. S1.

0.1. Photochemical tendencies from the Chapman+2 model

The photochemical tendencies in our idealized model come from a modified version of the Chapman Cycle, the classic model of ultraviolet photochemistry for O, O_2, and O_3 (Chapman, 1930). We augment the Chapman Cycle with two chemical reactions that represent additional damping of O and O_3 by catalytic reactions whose primary importance was not known when the Chapman Cycle was first formulated (Bates & Nicolet, 1950; Crutzen, 1970). The Chapman+2 model has been proposed along with a description of its tropical steady state in Match, Gerber, and Fueglistaler (2024b), whereas its sensitivity to perturbations has been explored in Match, Gerber, and Fueglistaler (2024a). The Chapman+2 reactions are:

$$\mathrm{O_2} + h\nu \rightarrow \mathrm{O} + \mathrm{O} \qquad (\lambda < 240\ \mathrm{nm}) \tag{R1}$$

$$\mathrm{O} + \mathrm{O_2} + M \ \rightarrow\ \mathrm{O_3} + \mathrm{M} \tag{R2}$$

$$\mathrm{O_3} + h\nu \ \rightarrow\ \mathrm{O_2} + \mathrm{O} \tag{R3}$$

$$\mathrm{O_3} + \mathrm{O} \ \rightarrow\ 2\mathrm{O_2} \tag{R4}$$

$$\mathrm{O} \ \rightarrow\ \frac{1}{2}\mathrm{O_2} \tag{R5}$$

$$\mathrm{O_3} \ \rightarrow\ \frac{3}{2}\mathrm{O_2} \tag{R6}$$

where R1-R4 is the classical Chapman Cycle, and R5-R6 are the two additional generalized sinks. R1 and R3 are photolysis reactions and M is a third body with the number density of air (n_a). The combination reactions proceed as the number density of the chemical reactants multiplied by a rate coefficient k_i, i=2,4, e.g., reaction 2 has a rate of $k_2[\mathrm{O}][\mathrm{O_2}][\mathrm{M}]$, which in general depends on temperature. The generalized reactions represent two sink pathways: destruction of odd oxygen can scale with atomic oxygen, as in R5 that proceeds at the rate $\kappa_{\mathrm{O}}[\mathrm{O}]$, or it can scale with ozone, as in R6 that proceeds at the rate $\kappa_{\mathrm{O_3}}[\mathrm{O_3}]$.

We solve the Chapman+2 chemical system by prognosing the long-lived chemical family of odd oxygen (O + $\mathrm{O_3}$) until it reaches a seasonally-evolving quasi-steady state, subject to the evolution equation:

$$\frac{\partial[\mathrm{O}_3]}{\partial t}|_{\mathrm{photochem}} = 2J_{\mathrm{O}_2}[\mathrm{O}_2] - 2k_4[\mathrm{O}][\mathrm{O}_3] - \kappa_{\mathrm{O}}[\mathrm{O}] - \kappa_{\mathrm{O}_3}[\mathrm{O}_3] \tag{2}$$

At each time-step [O] is solved diagnostically based on the fast partitioning between O and O_3 in the odd oxygen family (Match et al., 2024b):

$$[\mathrm{O}] = \frac{J_{\mathrm{O}_2} C_{\mathrm{O}_2} n_a + J_{\mathrm{O}_3}[\mathrm{O}_3] + \frac{\kappa_{\mathrm{O}_3}[\mathrm{O}_3]}{2}}{k_2 C_{\mathrm{O}_2} n_a^2 + \frac{\kappa_{\mathrm{O}}}{2}} \tag{3}$$

The photolysis rates J_{O_2} (s^{-1}) and J_{O_3} (s^{-1}) are governed by the spectrally-integrated UV absorption:

$$J_{\mathrm{O}_2}(z) = \int_{\lambda} q_{\mathrm{O}_2}(\lambda)\sigma_{\mathrm{O}_2}(\lambda) I_{\lambda}(z) d\lambda \tag{4}$$

$$J_{\mathrm{O}_3}(z) = \int_{\lambda} q_{\mathrm{O}_3}(\lambda)\sigma_{\mathrm{O}_3}(\lambda) I_{\lambda}(z) d\lambda \tag{5}$$

with wavelength λ, quantum yield $q_i(\lambda)$ (molecules decomposed per photon absorbed by species i), absorption coefficient σ_i (cm^2 molec^{-1}), and UV flux density with respect to wavelength $I_\lambda(z)$ (photons cm^{-2} s^{-1} nm^{-1}). The absorption of photons by photolysis attenuates the UV flux:

$$I_{\lambda}(z) = I_{\lambda}(\infty) \exp\left(-\frac{\tau_{\lambda}(z)}{\cos\theta}\right) \tag{6}$$

where $I_\lambda(\infty)$ is the incoming UV flux, θ is the solar zenith angle, and τ_λ is the optical depth as a function of wavelength. The optical depth at a given altitude depends on column-integrated O_2 and O_3 above that level:

$$\tau_\lambda(z) = \sigma_{\mathrm{O_2}}(\lambda)_{\mathrm{O_2}}(z) + \sigma_{\mathrm{O_3}}(\lambda)_{\mathrm{O_3}}(z) \tag{7}$$

where ${}_{\mathrm{O_2}} = \int_z^\infty [\mathrm{O_2}]dz$ and ${}_{\mathrm{O_3}} = \int_z^\infty [\mathrm{O_3}]dz$.

The collisional reaction rates k_2 and k_4 are calculated with temperature-dependent values from Brasseur and Solomon (2005). The generalized sinks of O and $\mathrm{O_3}$ proceed with damping rates representing catalytic cycles. Unlike in Match et al. (2024a, 2024b), which focused on the tropical stratosphere in which transport was parameterized through $\kappa_{\mathrm{O_3}}$, transport will be represented explicitly as a leaky tropical pipe. Catalytic cycles will be parameterized by taking all (temperature-dependent) damping-like terms from the budget of generalized odd oxygen ($\mathrm{O_y}$) of Brasseur and Solomon (2005), i.e., terms of the form $\partial \mathrm{O_y}/\partial t = -k[\mathrm{Z_O}][\mathrm{O}]$ are taken to damp O, and terms of the form $\partial \mathrm{O_y}/\partial t = -k[\mathrm{Z_{O_3}}][\mathrm{O_3}]$ are taken to damp $\mathrm{O_3}$, for catalysts $\mathrm{Z_O}$ and $\mathrm{Z_{O_3}}$. This leads to the following damping rates:

$$\kappa_{\mathrm{O}} = a_5[\mathrm{OH}] + a_7[\mathrm{HO_2}] + 2b_3[\mathrm{NO_2}] + 2d_3[\mathrm{ClO}] + 2e_3[\mathrm{BrO}] \tag{8}$$

$$\kappa_{\mathrm{O_3}} = a_2[\mathrm{H}] + a_6[\mathrm{OH}] + a_{6b}[\mathrm{HO_2}] \tag{9}$$

The Chapman+2 reactions are intended to provide only an idealized representation of the stratosphere, while excluding photochemical reactions among the catalysts, heterogeneous chemistry in the polar stratosphere, and tropospheric chemistry. Globally-average profiles of the catalysts will be prescribed based on output from the SOCRATES model tabulated in Brasseur and Solomon (2005).

0.2. Transport tendencies from the leaky tropical pipe model

The transport tendencies are represented as a leaky tropical pipe (Plumb, 1996; Neu & Plumb, 1999). The leaky tropical pipe considers the global transport by the Brewer-Dobson circulation and lateral two-way mixing, and we follow the treatment for ozone of Stolarski et al. (2014) and Match and Gerber (2022). The mass flux divergence of the upwelling in the tropics transports ozone to the extratropics. The tropics and extratropics have two-way lateral mixing on a timescale μ.

$$\frac{\partial[\mathrm{O_3}]_T}{\partial t}|_{\text{transport}} = -\frac{w_N + w_S}{A_f} n_a \frac{\partial}{\partial z}(\frac{[\mathrm{O_3}]_T}{n_a}) + \frac{\partial}{\partial z}(n_a K_T \frac{\partial}{\partial z}\frac{[\mathrm{O_3}]_T}{n_a}) - \frac{\mu}{A_f}([\mathrm{O_3}]_T - [\mathrm{O_3}]_N) - \frac{\mu}{A_f}([\mathrm{O_3}]_T - [\mathrm{O_3}]_S) \tag{10}$$

$$\frac{\partial[\mathrm{O_3}]_j}{\partial t}|_{\text{transport}} = w_j n_a \frac{\partial}{\partial z}(\frac{[\mathrm{O_3}]_j}{n_a}) + \frac{\partial}{\partial z}(n_a K_j \frac{\partial}{\partial z}\frac{[\mathrm{O_3}]_j}{n_a}) + (D_j + \mu)([\mathrm{O_3}]_T - [\mathrm{O_3}]_j) \tag{11}$$

where subscript T means tropics and subscript j means extratropics (j = S(outhern) or j = N(orthern)), A_f is the area of the tropical column divided by that of one of the extratropical columns, w_j is the rate of downwelling (units: m s^{-1}) in extratropical hemisphere j, μ is the lateral mixing rate between the tropics and extratropics (units: s^{-1}), and K is the vertical diffusivity (units: m^2 s^{-1}).

$$D_j = -e^{z/H}\frac{\partial}{\partial z}(w_j e^{-z/H}) \tag{12}$$

where $D_j(t)$ is the seasonally-varying mass flux divergence in hemisphere j of the downwelling (units: s^{-1}). We impose a sinusoidal seasonal cycle in the downwelling in each extratropical hemisphere (as in Stolarski et al., 2014):

$$w_j(t) = \overline{w_j}(1 + A_w \cos(\frac{2\pi t}{T_{year}} + \phi_j)) \tag{13}$$

where $\overline{w_j}$ is the annual average downwelling, A_w is the fractional annual cycle in downwelling, T_{year} is the period of the year, and ϕ_j is the phase shift of the annual cycle (ϕ_N = 0, $\phi_S = \pi$).

Text S2: Chapman+2 photochemical-transport model solution details

Our Chapman+2 photochemical-transport model unites and extends the photochemical treatment of Match et al. (2024b), which only considered a tropical column, and the transport treatment of Match and Gerber (2022), which represented a two-column leak tropical pipe, whereas we add a third column. Common among these solutions is our idealization of the atmosphere as being in a quasi-steady-state (now with a repeating annual cycle of the BDC), isothermal, and with a constant overhead sun angle (overhead in the tropics and 45° in the extratropics). We neglect scattering, clouds, and surface reflection. Eq. 1 is converged to a repeating seasonal cycle subject to zero ozone below the prescribed tropopause (default tropical tropopause of 17 km and extratropical tropopause of 10 km).

The vertical dimension is discretized into vertical levels ($\Delta z = 100$ meters) ranging from the surface to 100 km. The idealized shortwave radiative transfer and photolysis rates are solved on a wavelength grid with 621 discretized wavelengths ranging from 180 nm to 800 nm. Spectrally-resolved parameters are linearly interpolated to the wavelength grid. Solar UV flux is calculated from the Solar Spectral Irradiance Climate Data Record (Coddington et al., 2015), averaged from 01-01-2020 to 02-04-2021. O_2 absorption coefficients (σ_{O_2}) are taken from (Ackerman, 1971) and O_3 absorption coefficients (σ_{O_3}) from (Sander et al., 2010). The isothermal atmosphere has a default temperature of 240 K and scale height of 7 km. Temperature-dependent parameters for reaction rates $k_2(T)$ and $k_4(T)$ are taken from (Brasseur & Solomon, 2005).

Following Stolarski et al. (2014), we adopt a vertical diffusivity of $K_T = 0.01$ m^2 s^{-1} and $K_S = K_N = 0.5$ m^2 s^{-1}. Motivated by the isolation of the tropical pipe at high altitudes but the abundant mixing at low altitudes, we adopt a lateral mixing profile above the tropical tropopause of $\mu = 1$ year^{-1} and below the tropical tropopause of $\mu = 4$ year^{-1}. When the tropical tropopause shifts upward, this mixing profile also shifts upward, contributing to the upper dip.

The Chapman+2 model equilibrium is numerically converged to a repeating annual cycle, with results compared to a pre-industrial control experiment from MRI-ESM2-0 (Fig. S2). The Chapman+2 photochemical-transport model reproduces a reasonable vertical profile of ozone in each hemisphere and a realistic seasonal cycle, with extratropical lower stratospheric ozone peaking in the winter in each hemisphere. This realistic basic state gives confidence the model can be used to query the sensitivity to perturbations.

Data Set S1.

Movie S1.

Audio S1.

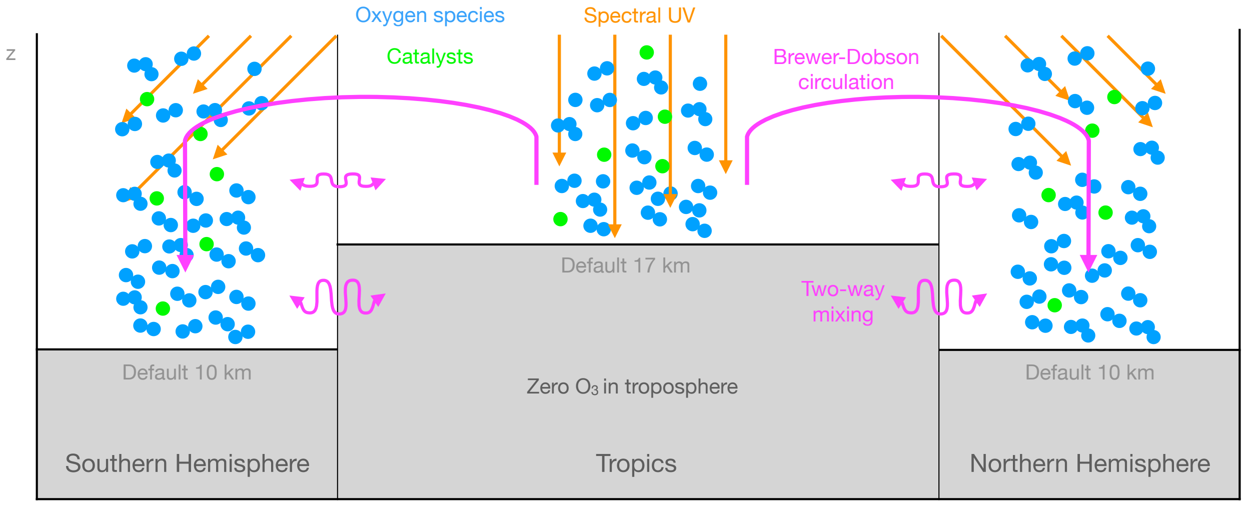

Figure S1. Schematic of the basic state model formulation for the Chapman+2 photochemical-transport model.

References

Ackerman, M. (1971). Ultraviolet Solar Radiation Related to Mesospheric Processes. In (pp. 149–159). Springer, Dordrecht. doi: 10.1007/978-94-010-3114-1_11

Bates, D. R., & Nicolet, M. (1950). The photochemistry of atmospheric water vapor. *Journal of Geophysical Research (1896-1977)*, *55*(3), 301–327. doi: 10.1029/JZ055i003p00301

Brasseur, G. P., & Solomon, S. (2005). *Aeronomy of the Middle Atmosphere: Chemistry and Physics of the Stratosphere and Mesosphere.* Dordrecht, Netherlands: Springer.

Chapman, S. (1930). A theory of upper atmospheric ozone. *Memoirs of the Royal Meteorological Society*, *III*(26), 103–125.

Coddington, O., Lean, J., Lindholm, D., Pilewskie, P., & Snow, M. (2015). *NOAA Climate Data Record (CDR) of Solar Spectral Irradiance (SSI), Version 2.1.* NOAA CDR Program. doi: 10.7289/V53776SW

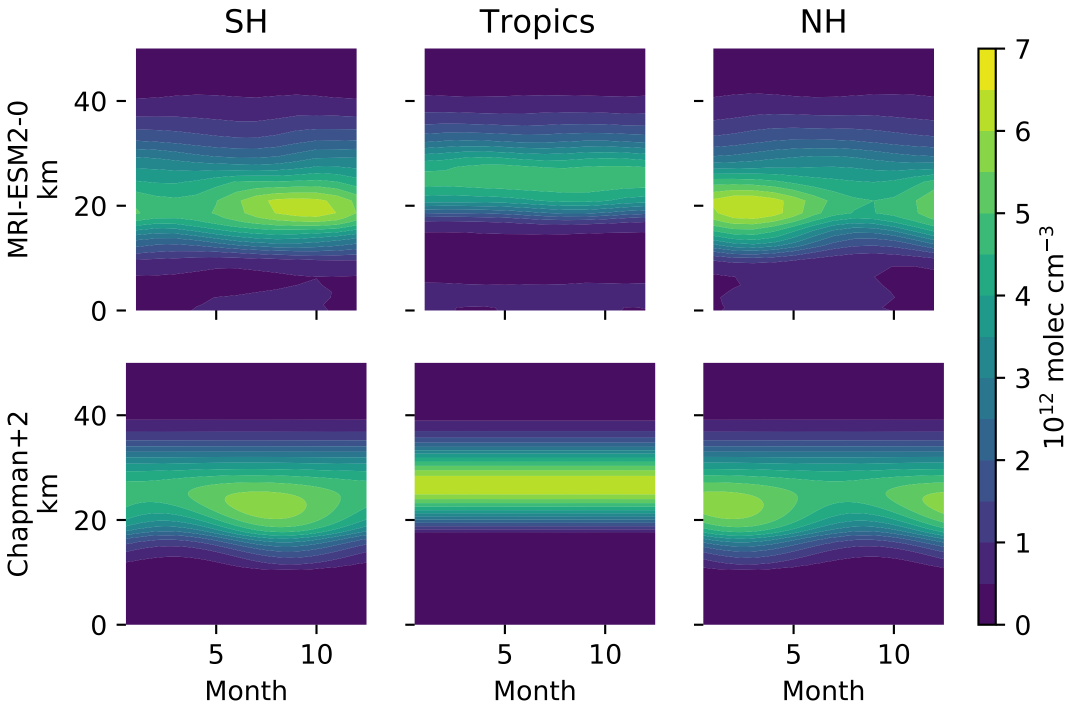

Figure S2. Validation of the Chapman+2 photochemical-transport model basic state and seasonal cycle. (Top row) Reference ozone seasonal cycle from MRI-ESM2-0 in the Southern Hemisphere extratropics (90°S-30°S), Tropics (30°S-30°N), and Northern Hemisphere extratropics (30°N-90°N). (Bottom row) Seasonal cycle in the Chapman+2 photochemical-transport model, in which the only seasonality arises from the prescribed Brewer-Dobson circulation, which maximizes on January 1 and minimizes on July 1. Despite its many idealization of the basic state and seasonal cycle, the Chapman+2 photochemical-transport model reproduces the basic vertical structure of ozone and its winter maximum and summer minimum in the extratropics.

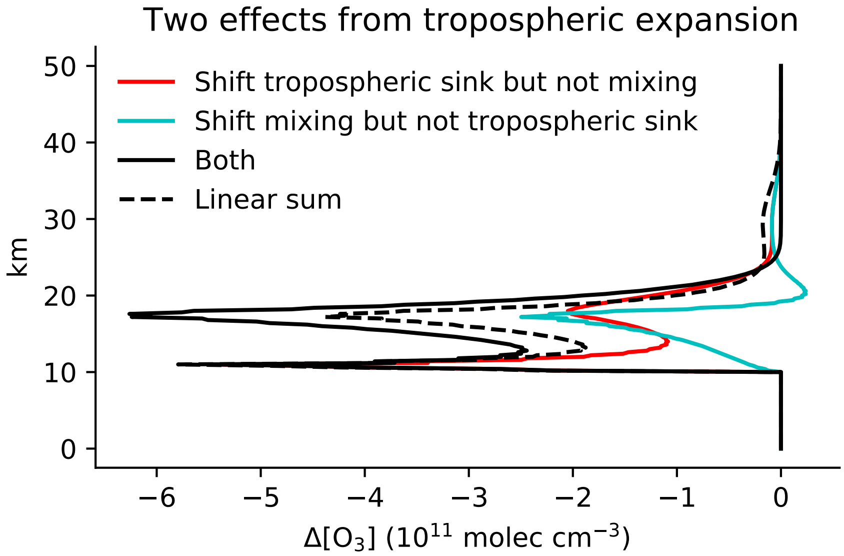

Figure S3. Decomposition of the responses to two processes that shift upwards under tropospheric expansion: tropospheric destruction of O_3 and lateral mixing. Both contribute approximately linearly to the resultant upper dip.

Crutzen, P. J. (1970, April). The influence of nitrogen oxides on the atmospheric ozone content. *Quarterly Journal of the Royal Meteorological Society*, *96*(408), 320–325. doi: 10.1002/qj.49709640815

Match, A., Gerber, E., & Fueglistaler, S. (2024a, January). Beyond self-healing: Stabilizing and destabilizing photochemical adjustment of the ozone layer. *EGUsphere*, 1–28. doi: 10.5194/egusphere-2024-147

Match, A., & Gerber, E. P. (2022, October). Tropospheric Expansion Under Global Warming Reduces Tropical Lower Stratospheric Ozone. *Geophysical Research Letters*, *49*(19), e2022GL099463. doi: 10.1029/2022GL099463

Match, A., Gerber, E. P., & Fueglistaler, S. (2024b, June). Protection without poison: Why tropical ozone maximizes in the interior of the atmosphere. *EGUsphere*, 1–29. doi: 10.5194/

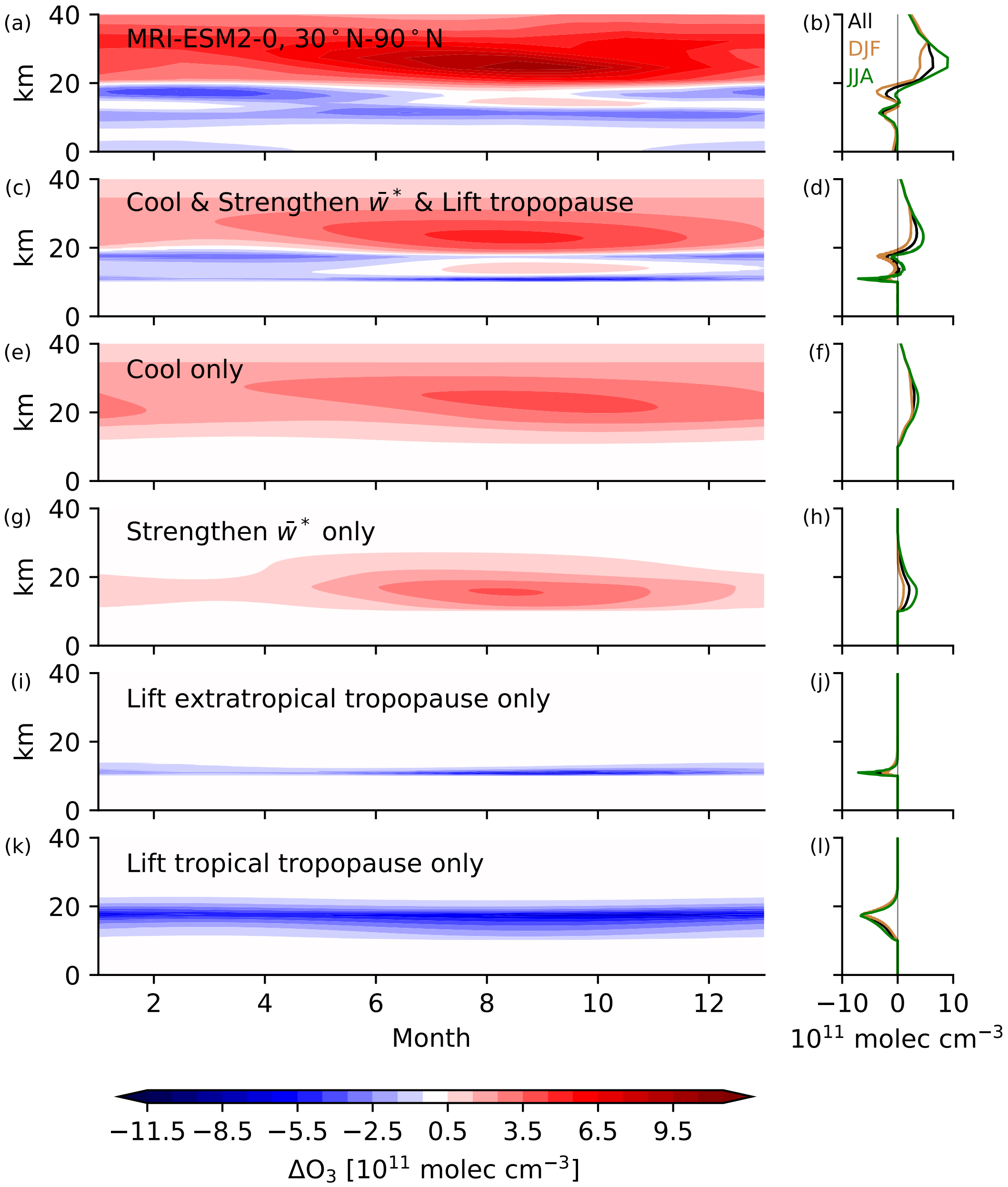

Figure S4. As in Figure 3 but for the Southern Hemisphere.

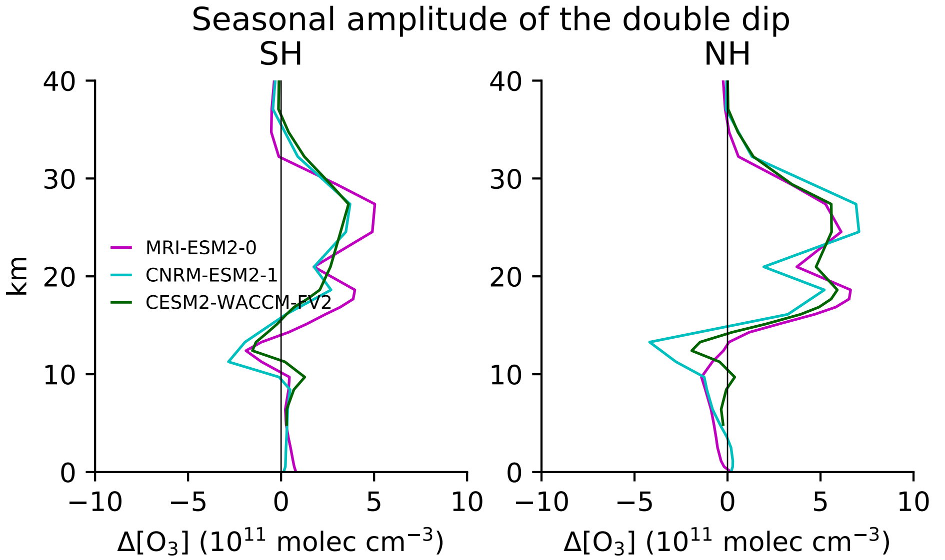

Figure S5. Seasonal cycle in the double dip (winter minus summer) in CMIP6 models in abrupt-4xCO2 (excluding first 50 years) minus piControl. (left) Southern Hemisphere (30°S-90°S) where winter = JJA and summer = DJF and (right) Northern Hemisphere (30°N-90°N) where winter = DJF and summer = JJA. The upper dip around 17 km is weakest in winter ($\Delta[O_3] > 0$), and the and the lower dip is strongest in winter ($\Delta[O_3] < 0$).

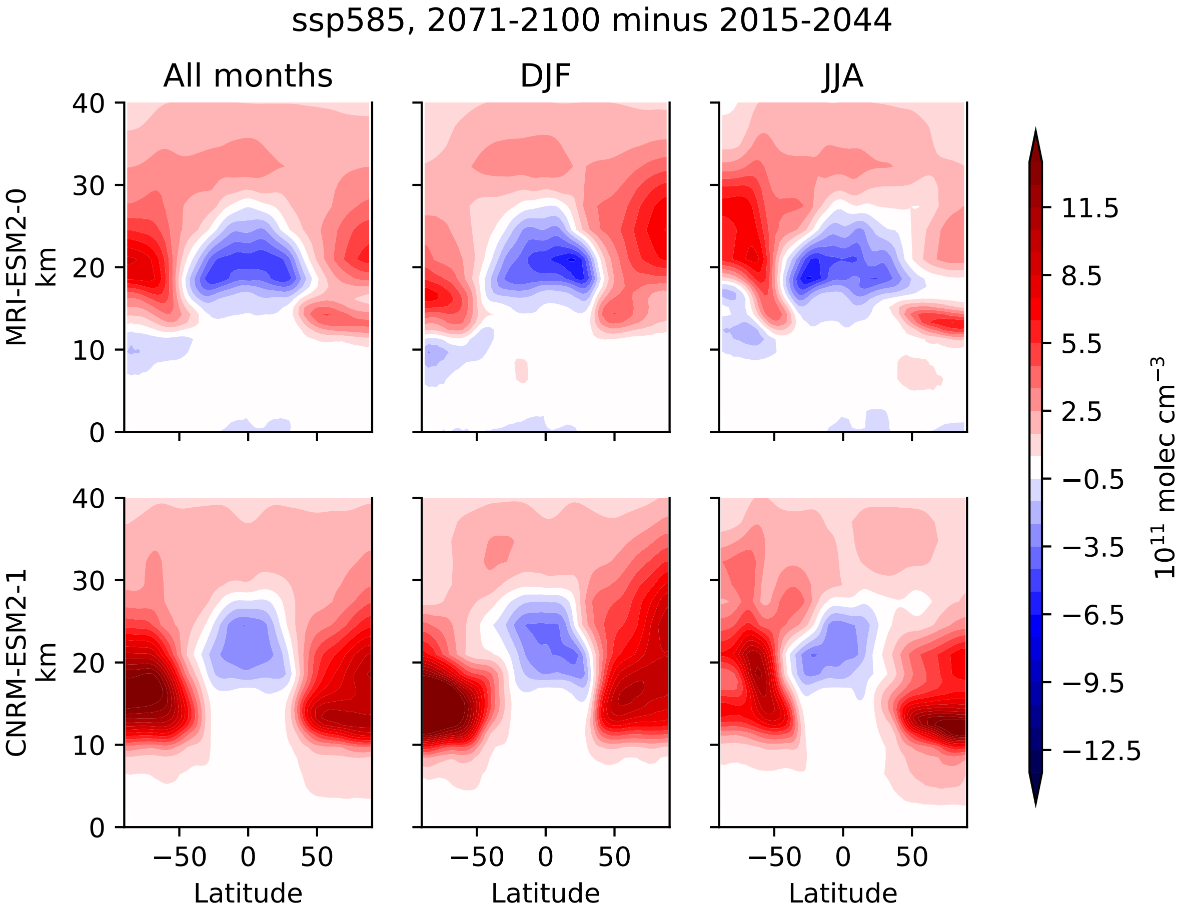

Figure S6. The ozone layer is not responding to rising CO_2 in isolation; the burden of ozone-depleting substances is also continuing to decline due to the Montreal Protocol. One future scenario for these two processes (and others that could affect the ozone layer) is captured by ssp585, an upper range for radiative forcing by 2100. The ozone difference between the latter part of the period (2071-2100) and the beginning (2015-2044) does not show strong evidence of a double dip, suggesting that the double dip is obscured by recovery from ozone-depleting substances. However, there is still an upper dip in the NH in MRI-ESM2-0, which is even more pronounced in JJA, and hints of an upper dip in the NH in CNRM-ESM2-1 in JJA.

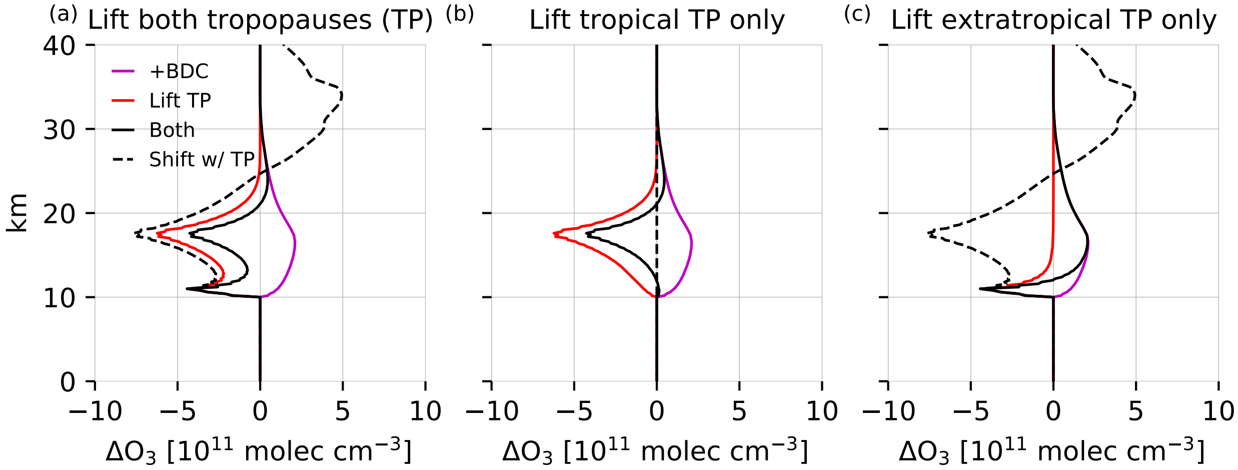

Figure S7. The extratropical ozone response to tropospheric expansion combines dynamical contributions from the local extratropical tropopause (responsible for the lower dip) and the nonlocal extratropical tropopause (responsible for the upper dip). The ozone response to lifting both the tropical and extratropical tropopauses (panel a) can be decomposed into a response to lifting only the tropical tropopause (panel b) or only the extratropical tropopause (panel c). Tropopause-following coordinates are justified to the extent that shifting the ozone layer along with the tropopause (dashed curve) reproduces the physical response to tropospheric expansion (black curve, or arguably the red curve if the effect of the strengthening BDC is excluded). The upward shift of the tropopause roughly reproduces the ozone response when the tropopauses shift together, but when the extratropical and tropical tropopauses shift by different amounts, an upward shift along with extratropical tropopause fails to reproduce the actual ozone change (panels b&c, black dashed versus solid curves).

egusphere-2024-1552

Neu, J. L., & Plumb, R. A. (1999, August). Age of air in a "leaky pipe" model of stratospheric transport. *Journal of Geophysical Research*, *104*(D16), 19243. doi: 10.1029/1999JD900251

Plumb, R. A. (1996, February). A "tropical pipe" model of stratospheric transport. *Journal of Geophysical Research*, *101*(D2), 3957. doi: 10.1029/95JD03002

Sander, S. P., Abbatt, J., Barker, J. R., Burkholder, J. B., Friedl, R. R., Golden, D. M., … Wine, P. H. (2010). *Chemical Kinetics and Photochemical Data for Use in Atmospheric Studies, Evaluation No. 17* (Tech. Rep. No. 10-6). Pasadena, CA: Jet Propulsion Laboratory.

Stolarski, R. S., Waugh, D. W., Wang, L., Oman, L. D., Douglass, A. R., & Newman, P. A. (2014, May). Seasonal variation of ozone in the tropical lower stratosphere: Southern tropics are different from northern tropics. *Journal of Geophysical Research: Atmospheres*, *119*(10), 6196–6206. doi: 10.1002/2013JD021294